



## Phenomenological approach of the thermodynamic properties of the charge density wave systems

M. Saint-Paul & P. Monceau

To cite this article: M. Saint-Paul & P. Monceau (2020): Phenomenological approach of the thermodynamic properties of the charge density wave systems, Philosophical Magazine, DOI: [10.1080/14786435.2020.1844917](https://doi.org/10.1080/14786435.2020.1844917)

To link to this article: <https://doi.org/10.1080/14786435.2020.1844917>



Published online: 20 Nov 2020.



Submit your article to this journal [↗](#)



Article views: 29



View related articles [↗](#)



View Crossmark data [↗](#)



# Phenomenological approach of the thermodynamic properties of the charge density wave systems

M. Saint-Paul and P. Monceau

Université Grenoble Alpes Grenoble INP, Institut Néel, Grenoble, France

## ABSTRACT

The properties of the specific heat and elastic stiffness components at the charge density wave phase transition in several one-dimensional and two-dimensional materials are examined. Here we show that the thermodynamic properties of the rare earth tritelluride  $R\text{Te}_3$  ( $R = \text{Te}, \text{Er}$ ) and  $\text{Lu}_5\text{Ir}_4\text{Si}_{10}$  compounds can be explained in the framework of a standard mean field Landau theory. The amplitude of the experimental-specific heat jump measured at the charge density wave (CDW) phase transition increases with the transition temperature  $T_{\text{CDW}}$ . The amplitude of the experimental discontinuity of the longitudinal elastic constants measured at the CDW phase transition scales onto a single curve. The Landau approach is discussed as well as experimental results.

## ARTICLE HISTORY




Received 21 April 2020  
Accepted 25 September 2020

## KEYWORDS

Charge density wave;  
specific heat; elastic  
constants

## 1. Introduction

The concept of a charge density waves (CDWs) which is induced by Fermi surface nesting originated from the Peierls idea of electronic instabilities in purely one-dimensional system is now often applied to charge ordering in real low dimensional materials [1–60]. The microscopic origin of the CDW phase transition is still debated and remains controversial [6,7]. Physical CDW phenomenon has attracted a great interest in condensed matter physics. In general, a real material does not go through a pure metal insulator transition at  $T_{\text{CDW}}$  and implies a partial gapping of the Fermi surface. The claim that this transition is CDW by the community needs to be completely rethought [6,7]. The question is how to extend the Peierls picture to real systems. Historically, CDWs have been associated with instabilities of quasi-one-dimensional metals. But instabilities have been recognised to develop in three-dimensional materials which involve strong electronic correlations [8]. Many materials have been classified as CDW materials without a clear definition of the underlying nature of their CDW states. Four types of CDW have been proposed in [6,7]:

**CONTACT** M. Saint-Paul  michel.saint-paul@neel.cnrs.fr; P. Monceau  pierre.monceau@neel.cnrs.fr  Univ Grenoble Alpes Grenoble INP, Institut Néel, 25 Avenue des Martyrs, Grenoble, France

- (1) Type I, CDW in one-dimensional conductors have their origin in the Peierls mechanism such as  $K_{0.3}MoO_3$ ,  $NbSe_3$ , TTF-TCNQ,  $TaS_3$ ,  $(TaSe_4)_2I$  [3,9–14]. In a strictly one-dimensional material with short-range interactions, there are no phase transition at finite temperature because fluctuations destroy long-range order. A finite-temperature transition only occurs as a result of interchain interactions and Landau theory should describe with a two-component order parameter the ordering transition of a quasi-one-dimensional system.
- (2) Type II, CDW in two-dimensional materials: Transition metal dichalcogenides (TMD) have been the centre of CDW research since several decades but the results are still confusing [15–20]. TMD are quasi-two-dimensional materials exhibiting a wide variety of properties that are both fundamental and applied interest. Transitions in the TMD are not CDW in the sense of a Peierls picture; even in these layered materials they are in some cases 3D in nature. TMD  $2H-NbSe_2$  is known to be an archetype-layered TMD with a superconducting transition temperature of 7.3 K. Quasi-two-dimensional layered TMD have been the subject of intense research owing to their rich electronic properties resulting from lower dimensionality.  $1T-TiSe_2$  undergoes a second-order phase transition to a commensurate lattice distortion  $2 \times 2 \times 2$ . Some authors described  $TiSe_2$  as a CDW transition [19,20]. In fact this transition is a commensurate structural transition which induces periodic charge modulation.

The family of rare earth tritellurides  $RTe_3$ , R being an element of the Lanthanide group is a model of a two-dimensional charge density system. The origin of CDW in  $RTe_3$  is related to the momentum-dependent electron phonon coupling [21–24].  $RTe_3$  are quasi-two-dimensional metals where a clearer situation is encountered. The electronic structure is more simple being built by broad p-type bands of Te atoms [21–25].

Rare earth tritellurides compounds  $TbTe_3$ ,  $ErTe_3$  and  $HoTe_3$  have been studied intensively [21–28].

The  $RTe_3$  compounds crystallise in the orthorhombic structure described by the  $Cmcm$  space group. Lattice consists of stacked Te layers alternating with  $RTe$  layers with unit cell with a large anisotropy in the lattice parameters  $a \approx c \approx 4 \text{ \AA}$  and  $b \approx 25 \text{ \AA}$  [23]. The CDW in  $RTe_3$  is characterised by large displacements and large gap in the electronic structure. Periodic lattice distortions are associated with the presence of an incommensurate CDW along both the  $\vec{a}$  and  $\vec{c}$  crystallographic axes shown by electron diffraction. The incommensurate lattice modulation has a unidirectional wavevector  $q_1 = (2/7)c^*$  ( $c^* = 2\pi/c$ ) at the upper CDW phase transition and the wavevector  $q_2 = (1/3)a^*$  ( $a^* = 2\pi/a$ ) is perpendicular to the first wavevector  $q_1$  at the lower CDW phase transition which occurs with heavy rare earth atoms.

- (3) Type III, CDW in three-dimensional materials: The origin of CDW in three dimensional materials is not yet well defined. The intermetallic compound  $\text{Lu}_5\text{Ir}_4\text{Si}_{10}$  exhibits a weakly first-order (small thermal hysteresis of 1 K) CDW transition at  $T_{\text{CDW}} \approx 80$  K associated with a commensurate lattice modulation along the  $c$  axis with a seven-unit cell period [29–37]. Rare earth compounds of the type  $\text{Lu}_5\text{Ir}_4\text{Si}_{10}$  display various ground states, charge density waves and superconductivity [31,32]. The competition between CDW and superconductivity was demonstrated through the observation of enhanced superconductivity upon suppression of the CDW by pressure  $\text{Lu}_5\text{Ir}_4\text{Si}_{10}$  [31]. The same pressure dependence is observed on the superconducting and CDW phase transitions which gives a strong evidence for the involvement of the Fermi surface. X-rays revealed in  $\text{LaAgSb}_2$  a development of periodic lattice modulation along the  $\vec{a}$  axis at the upper CDW phase transition at 210 K and an additional ordering along the  $\vec{c}$  axis at the lower CDW phase transition at 185 K [35]. Finally, the mechanism responsible for the CDW state found in  $\text{Fe}_3\text{O}_2\text{BO}_3$  is different from that of the Peierls mechanism and is related with excitonic instabilities [36,37].  $\text{Fe}_3\text{O}_2\text{BO}_3$  belongs to the family of the oxyborates and is characterised by the presence of low-dimensional units in the form of ladders along the  $\vec{c}$ -axis. This material presents a structural transition concomitant with the charge ordering of itinerant electrons in the rungs of the ladders. This transition is associated with the formation of a CDW. The CDW observed by Mössbauer spectroscopy is associated with atomic displacements transverse to the direction of the ladders.

Instabilities in the Fermi surface can lead to ground states such as spin density wave (SDW) in pure three-dimensional Cr [38–46]. Below 312 K the electrons form a SDW with a period which is incommensurable with the lattice. The properties of Cr is surveyed by Fawcett [41]. The transition to the SDW state at the Néel temperature in Cr was explained by Walker [40] using a Landau theory with an order parameter related to the components of the SDW polarisation vector.

- (4) Type IV, CDW in cuprates: Recently, the competition between CDWs and superconductivity was observed in superconducting cuprates where CDWs emerge when superconductivity is weakened by a magnetic field [47].

The elastic constants are thermodynamic derivatives. They are important together with the specific heat and thermal expansion for the equation of state of a material [48–50]. The purpose of this paper is to examine the experimental specific heat results and the measurements of the elastic stiffness components at the CDW phase transition in the rare earth tritellurides  $\text{TbTe}_3$ ,  $\text{ErTe}_3$ ,  $\text{HoTe}_3$  and the compound  $\text{Lu}_5\text{Ir}_4\text{Si}_{10}$ . The experimental

data are analysed in the framework of a phenomenological Landau approach [51–54]. As we show below, it appears that CDW transitions in several materials can be described with similar parameters in the mean field approximation [1]. The amplitude of the specific heat jump at the CDW transition increases linearly with increasing phase transition temperature  $T_{\text{CDW}}$ . In the same manner, the amplitude of the discontinuity of the velocity of the longitudinal mode increases with increasing  $T_{\text{CDW}}$ , in fact a quadratic dependence is observed. Landau theory can successfully explain the mean field character of a phase transition but when  $T$  is sufficiently close to the phase transition temperature the contribution related to fluctuations is comparable to the mean field discontinuity, the critical regions are given by the Ginsburg criterion [1,3,10]. Departures of the thermodynamic properties from the mean field behaviour at the CDW phase transition are attributed to fluctuations which belong to the 3D XY criticality class [1,55,56].

## 2. Thermodynamic properties

### 2.1. Landau theory of a second-order phase transition

The physics of quasi-one-dimensional solids which undergo a Peierls transition was discussed in terms of a phenomenological Landau approach by McMillan for the CDWs in TMDs with the CDW as an order parameter [42–44]. The quantities of interest are the temperature at which the transition  $T_{\text{CDW}}$  occurs and the order parameter  $Q$ . The widespread use of Landau theory for analysing incommensurate phases has produced a voluminous literature [57]. Landau theory in its simplest form starts with a free energy  $F$  of the system expressed as a power series expansion in the order parameter  $Q$  in the mean field approximation at a second-order phase transition:

$$F(Q, T)_0 = F(0, T)_0 + (1/2)a(T - T_{\text{CDW}})Q^2 + (1/4)cQ^4 \quad (1)$$

where the coefficients  $a$  and  $c$  are to be estimated. The order parameter that minimises the free energy in Equation (1) ( $\frac{\partial F}{\partial Q} = 0$ ) is

$$Q = \sqrt{\frac{a}{c}} \sqrt{T_{\text{CDW}} - T} \quad (2)$$

The order parameter  $Q(0)$  can be normalised to 1 at 0 K and gives the relation

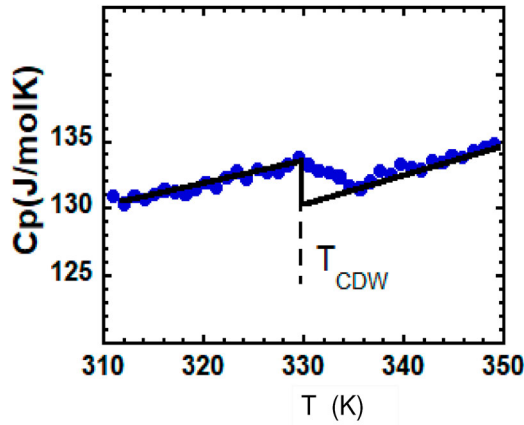
$$Q(0)^2 = \frac{a}{c} T_{\text{CDW}} \quad (3a)$$

$$c = aT_{\text{CDW}} \quad (3b)$$

There is a specific heat jump  $\Delta C_p$  at a second-order phase transition (Table 1). An example (TbTe<sub>3</sub>) is shown in Figure 1. The specific heat jump

**Table 1.** Materials; molar volumes given in  $\text{m}^3$ ; phase transition temperatures; specific heat jumps; velocity discontinuities.

Materials molar vol.	Materials	
	$T_{\text{CDW}}$ $\Delta C_p$	Elastic modulus velocity discont.
$\text{K}_{0.3}\text{MoO}_3$	180 K	$Y = 250 \text{ GPa}$
$3.5 \times 10^{-5} \text{ m}^3$	$3 \text{ J mol}^{-1} \text{ K}^{-1}$ [10]	$\Delta V_Y/V_Y = 0.01$ [10]
$\text{NbSe}_3$	145 K	
$4.1 \times 10^{-5} \text{ m}^3$	$0.3 \text{ J mol}^{-1} \text{ K}^{-1}$	$\Delta V/V = 0.0005$ [15]
$(\text{TaSe}_4)_2\text{I}$	260 K	$C_{33}$
$7.8 \times 10^{-5} \text{ m}^3$	$0.8 \text{ J mol}^{-1} \text{ K}^{-1}$	$\Delta V_{33}/V_{33} = 0.001$ [3]
TTF-TCNQ	55 K	$Y = 60 \text{ GPa}$
$2.5 \times 10^{-4} \text{ m}^3$	$2.5 \text{ J mol}^{-1} \text{ K}^{-1}$	$\Delta V_Y/V_Y = 0.01$ [14]
2H-TaSe <sub>2</sub>	120 K	$C_{11} = 120 \text{ GPa}$
$3.9 \times 10^{-5} \text{ m}^3$	$4 \text{ J mol}^{-1} \text{ K}^{-1}$ [12]	$\Delta V_{11}/V_{11} = 0.0005$
2H-NbSe <sub>2</sub>	30 K	$C_{11} = 108 \text{ GPa}$
$4 \times 10^{-5} \text{ m}^3$	$0.5 \text{ J mol}^{-1} \text{ K}^{-1}$ [16]	$\Delta V_{11}/V_{11} = 0.0005$ [17]
TiSe <sub>2</sub>	200 K	$C_{33} = 120 \text{ GPa}$
$4 \times 10^{-5} \text{ m}^3$	$1 \text{ J mol}^{-1} \text{ K}^{-1}$ [21]	$\Delta V_{33}/V_{33} = 0.05$ [20]
TbTe <sub>3</sub>	330 K	$C_{33} = 50 \text{ GPa}$
$7.1 \times 10^{-5} \text{ m}^3$	$3 \text{ J mol}^{-1} \text{ K}^{-1}$ [26]	$\Delta V_{33}/V_{33} = 0.01$ [26]
ErTe <sub>3</sub>	260 K	$C_{33} = 50 \text{ GPa}$
$7 \times 10^{-5} \text{ m}^3$	$1 \text{ J mol}^{-1} \text{ K}^{-1}$ [27]	$\Delta V_{33}/V_{33} = 0.015$ [28]
HoTe <sub>3</sub>	280 K	$C_{33} = 50 \text{ GPa}$
$7 \times 10^{-5} \text{ m}^3$		$\Delta V_{33}/V_{33} = 0.025$ [28]
$\text{Lu}_5\text{Ir}_4\text{Si}_{10}$	80 K	$C_{11} = 230 \text{ GPa}$
$2 \times 10^{-4} \text{ m}^3$	diverges [32]	$\Delta V_{11}/V_{11} = 0.005$ [34]
$\text{LaAgSb}_2$	210 K	
$6.3 \times 10^{-5} \text{ m}^3$	$0.5 \text{ J mol}^{-1} \text{ K}^{-1}$ [35]	
$\text{Fe}_3\text{O}_2\text{BO}_3$	290 K	
$5 \times 10^{-5} \text{ m}^3$	$15 \text{ J mol}^{-1} \text{ K}^{-1}$ [36]	
Cr	310 K	$C_{33} = 400 \text{ GPa}$
$7.2 \times 10^{-6} \text{ m}^3$	$3 \text{ J mol}^{-1} \text{ K}^{-1}$ [38]	$\Delta V_{33}/V_{33} = 0.05$ [39]

**Figure 1.** Specific heat jump at the CDW phase transition in  $\text{TbTe}_3$ , data taken from [26]. (Colour online)

$\Delta C_P$  deduced from Equation (1) is given by

$$S = -\frac{\partial F}{\partial T} \quad (4)$$

$$\frac{\Delta C_P}{V_m T} = \frac{\partial S}{\partial T} \quad (5)$$

$$\frac{\Delta C_P}{V_m} = \frac{a^2}{2c} T_{\text{CDW}} \quad (6)$$

where  $V_m$  is the molar volume. The order parameter is defined by the energy gap  $\Delta$  in the one-dimensional chain model of Allender et al. [45] and the Landau parameters  $a'$  and  $c'$  are given by:

$$F(\Delta, T)_0 = F(0, T)_0 + (1/2)a'(T - T_{\text{CDW}})\Delta^2 + (1/4)c'\Delta^4 \quad (7a)$$

$$a' = N(E_F)/T_{\text{CDW}}; \quad c' = 0.1N(E_F)/(k_B^2 T_{\text{CDW}}^2) \quad (7b)$$

At 0 K the order parameter  $\Delta(0)$  is related to the parameters  $a'$  and  $c'$

$$\Delta(0)^2 = \frac{a'}{c'} T_{\text{CDW}} \quad (8a)$$

$$\Delta(0)^2 = 10k_B^2 T_{\text{CDW}}^2 \quad (8b)$$

The amplitude of the specific heat anomaly calculated in the Allender et al. model increases linearly with increasing  $T_{\text{CDW}}$  as expected at a second order phase transition, Equation (6) is similar to the BCS relation [1,42–44].

$$\Delta C_P/V_m \approx 10N_0N(E_F)k_B^2 T_{\text{CDW}} \quad (9)$$

$N_0$  is the Avogadro number. Similar values of  $N(E_F)$  are found in the CDW

**Table 2.** Fermi energy  $E_F$ , density of states at the Fermi level  $N(E_F)$  (u.c. =unit cell).

Materials		
$\text{K}_{0.3}\text{MoO}_3$	$T_{\text{CDW}} = 180 \text{ K}$	$E_F \approx 0.24 \text{ eV}$ [1] $N(E_F) \approx 3 \text{ states/eV u.c.}$
$\text{NbSe}_3$	$T_{\text{CDW}} = 145 \text{ K}$	$E_F \approx 0.1 \text{ eV}$ [1] $N(E_F) \approx 2 \text{ states/eV u.c.}$
$(\text{TaSe}_4)_2\text{I}$	$T_{\text{CDW}} = 260 \text{ K}$	$E_F \approx 0.7 \text{ eV}$ [1] $N(E_F) \approx 1.3 \text{ states/eVu.c.}$
TTF-TCNQ	$T_{\text{CDW}} = 55 \text{ K}$	$E_F \approx 0.2 \text{ eV}$ [8] $N(E_F) \approx 3 \text{ states/eV u.c.}$
2H-TaSe <sub>2</sub>	$T_{\text{CDW}} = 120 \text{ K}$	$E_F \approx 0.6 \text{ eV}$ [8] $N(E_F) \approx 5 \text{ states/eV u.c.}$
TiSe <sub>2</sub>	$T_{\text{CDW}} = 200 \text{ K}$	$E_F \approx 0.2 \text{ eV}$ [8] $N(E_F) \approx 1 \text{ states/eV u.c.}$
TbTe <sub>3</sub>	$T_{\text{CDW}} = 330 \text{ K}$	$N(E_F) \approx 1.5 \text{ states/eV u.c.}$ [23]
$\text{Lu}_5\text{Ir}_4\text{Si}_{10}$	$T_C = 80 \text{ K}$	$N(E_F) \approx 0.26 \text{ states/eV atom}$ [30]

materials (Table 2). In the case of a spin density wave, the thermodynamic quantities near  $T_{\text{SDW}}$  can be described in terms of the Landau theory which follows the description of the charge density wave [1,42–44]. As for a CDW the development of the SDW ground state opens up a gap at the Fermi level leading to a metal insulator transition [1,22,40–46]. The interpretation of the elastic constant at second order phase transition is based on an expansion of the free energy density in powers of the strain components developed by Rhewald [51]. Considering here specifically the  $R\text{Te}_3$  compounds the expansion is limited to the longitudinal strains  $e_1$  and  $e_3$  along the in-plane crystallographic  $\vec{a}$  and  $\vec{c}$  axes and Equation (1) is modified:

$$F(\Delta, T, e_1, e_3) = F(\Delta, T)_0 + (1/2)C_{11,0}e_1^2 + (1/2)C_{33,0}e_3^2 + g'_1e_1\Delta^2 + g'_3e_3\Delta^2 + h'_1e_12\Delta^2 + h'_3e_3^2\Delta^2 \quad (10)$$

where  $(1/2)C_{11,0}e_1^2 + (1/2)C_{33,0}e_3^2$  is the elastic background energy at  $\Delta = 0$  and  $g'_1$ ,  $g'_3$ ,  $h'_1$  and  $h'_3$  are the coupling constants. At a CDW phase transition the longitudinal strain components couple with the square of the order parameter. The new elastic constant are given by

$$C_{11} = C_{11,0} - (d^2F/d\Delta de_1)^2\chi_\Delta \quad (11a)$$

$$C_{33} = C_{33,0} - (d^2F/d\Delta de_3)^2\chi_\Delta \quad (11b)$$

where  $\chi_Q$  denotes the order parameter susceptibility [51]

$$\chi_\Delta = (d^2F/d\Delta^2)^{-1} \quad (12)$$

Finally the new elastic constant are given by

$$C_{11} \approx C_{11,0} - 2g_1'^2/c' \quad (13a)$$

$$C_{33} \approx C_{33,0} - 2g_3'^2/c' \quad (13b)$$

It results that a decrease of the elastic constants  $C_{11}$  and  $C_{33}$  occurs at a second-order phase transition. The behaviours of the elastic constant  $C_{33}$  observed at the CDW phase transition in  $\text{TbTe}_3$  (Figure 2),  $\text{ErTe}_3$  (Figure 3) and  $\text{HoTe}_3$  (Figure 4) are shown. The coefficient  $c'$  in the Allender model (Equation (7b)) varies as  $c'^{-1} \approx T_{\text{CDW}}^2$ . It results that the discontinuity of the elastic constant increases as the square of the temperature  $T_{\text{CDW}}$ . In summary, in the Allender model [45], at the CDW phase transition the specific heat jump  $\Delta C_P/V_m$  increases as  $T_{\text{CDW}}$  (Equation (10)) and the elastic constant discontinuity  $\Delta C_{11}$  or  $\Delta C_{33}$  increases as  $T_{\text{CDW}}^2$ .

In general the effect of a phase transition on the elastic constants in any second-order phase transition can be calculated from the derivative of the strain dependence of the transition temperature  $T_{\text{CDW}}$  using the Ehrenfest



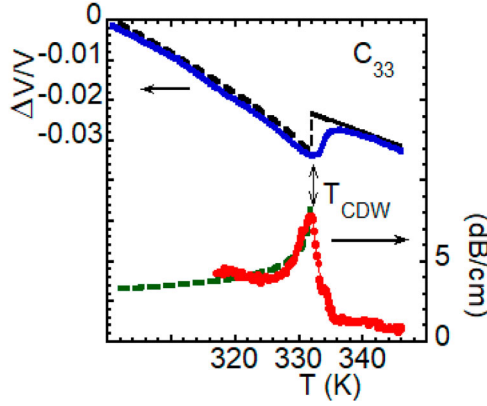


**Figure 2.** Velocity discontinuity ( $V_{33}$ ) and attenuation (dB/cm) of the longitudinal  $C_{33}$  mode at the CDW phase transition in  $\text{TbTe}_3$ . The dashed (green) curve is calculated using  $\text{Att} = 6\omega\tau_{\text{LK}}/(1 + (\omega\tau_{\text{LK}})^2)$  with  $\tau_{\text{LK}} = 2 \times 10^{-12}\{(332 - T)/332\}^{-1}$  s at frequency  $\omega/2\pi = 15$  MHz, data taken from [26]. (Colour online)

relations reformulated by Testardi [50]. In the anisotropic case for a strain component  $e_1$  along the crystallographic  $\vec{a}$  direction the change in the elastic stiffness  $C_{11}$  is given by the logarithmic derivative of  $T_{\text{CDW}}$ .

$$\Delta C_{11} = \frac{\Delta C_P T_{\text{CDW}}}{V_m} [d(\ln(T_{\text{CDW}}))/de_1]^2 \quad (14)$$

It results that the discontinuity in the elastic stiffness component increases linearly with  $\Delta\gamma = \Delta C_P/T_{\text{CDW}}$  and is proportional to the square of the phase

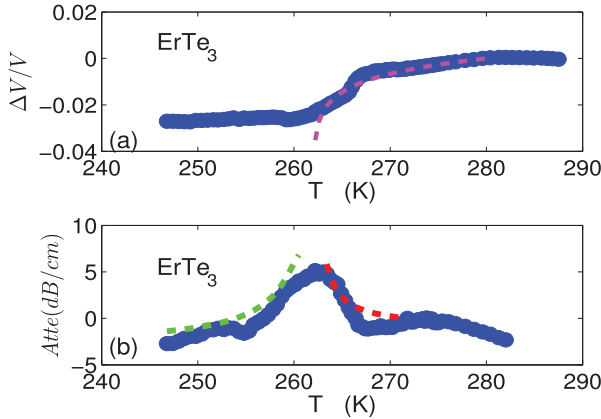


**Figure 3.** (a) Velocity decrease ( $V_{11}$ ) of the longitudinal  $C_{11}$  mode at the CDW phase transition in  $\text{ErTe}_3$ . The dashed (pink) curve is calculated using  $\Delta V/V = 0.319 - 0.342\{(T - 262)/262\}^{0.026}$ . (b) Attenuation of the  $C_{11}$  mode. The dashed (green) curve is calculated using  $\text{Att} = 20\omega\tau_{\text{LK}}/(1 + (\omega\tau_{\text{LK}})^2)$  with  $\tau_{\text{LK}} = 5 \times 10^{-11}\{(262 - T)/262\}^{-1}$  s. The dashed (red) curve is calculated with  $\text{Att} = 40\omega\tau_f/(1 + (\omega\tau_f)^2)$  with  $\tau_f = 1 \times 10^{-11}\{(T - 262)/262\}^{-1}$  s at frequency  $\omega/2\pi = 15$  MHz, data taken from [27]. (Colour online)

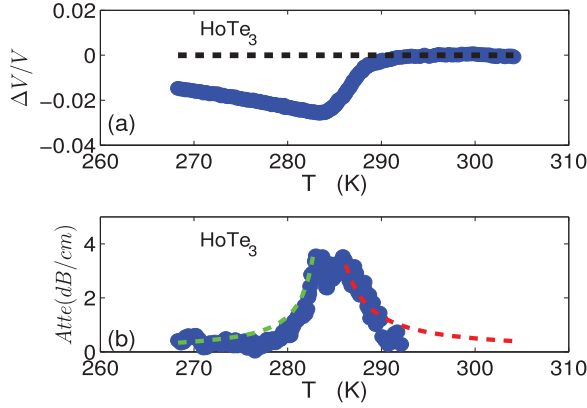


**Figure 4.** (a) Velocity decrease ( $V_{33}$ ) of the longitudinal  $C_{33}$  mode at the CDW phase transition in  $\text{HoTe}_3$ . (b) Attenuation of the  $C_{33}$  mode. The dashed (green) curve is calculated using  $\text{Att} = 10\omega\tau_{\text{LK}}/(1 + (\omega\tau_{\text{LK}})^2)$  with  $\tau_{\text{LK}} = 2 \times 10^{-11}\{(284 - T)/284\}^{-1}$  s the dashed (red) curve is calculated using  $\text{Att} = 10\omega\tau_{\text{F}}/(1 + (\omega\tau_{\text{F}})^2)$  with  $\tau_{\text{F}} = 3 \times 10^{-11}\{(T - 284)/284\}^{-1}$  s at frequency  $\omega/2\pi = 15$  MHz, data taken from [28]. (Colour online)

transition  $T_{\text{CDW}}$  because the logarithmic derivative of the strain dependence of  $T_{\text{CDW}}$  does not change very much with  $T_{\text{CDW}}$  [22].

$$\Delta C_{11} = \frac{\Delta\gamma T_{\text{CDW}}^2}{V_m} [d(\ln(T_{\text{CDW}}))/de_1]^2 \quad (15)$$

Finally below  $T_{\text{CDW}}$  in the ordered phase, consequently to the coupling terms  $h'_1 e_1^2 Q^2 + h'_3 e_3^2 Q^2$ , the temperature dependence of the elastic constants  $C_{11}$  and  $C_{33}$  (or velocity) follows the temperature dependence of the order parameter (black dotted curve in Figure 2) as explained in [51]:

$$C_{11} \approx h'_1 Q^2 \quad \text{and} \quad C_{33} \approx h'_3 Q^2 \quad (16)$$

## 2.2. Landau theory of a first order phase transition

A cubic term is included in the expansion of the free energy in case of a first order phase transition [42–44,49]. The third-order term in Equation (1) is discussed by Moncton et al. [58] in the case of 2H-TaSe<sub>2</sub> and 2H-NbSe<sub>2</sub>. There is a third-order term only in the case of a commensurate CDW phase. The requirement between the three wavevectors involved in the Umklapp process associated with the third-order term is satisfied for a commensurate CDW wave but not for an incommensurate wave. This condition is verified at the phase transition in Lu<sub>5</sub>Ir<sub>4</sub>Si<sub>10</sub> where a commensurate lattice modulation of seven unit cells is observed [33].

For a tetragonal-symmetry system (crystallographic axes  $\vec{a} = \vec{b}$  and  $\vec{c}$ ) such as Lu<sub>5</sub>Ir<sub>4</sub>Si<sub>10</sub> [29–31] there are two independent longitudinal elastic constants

$C_{11} = C_{22}$  and  $C_{33}$ . The Landau free energy has the form:

$$F(Q, T, e_1, e_3) = F(0, T)_0 + (1/2)a(T - T_0)Q^2 - (1/3)bQ^3 + (1/4)cQ^4 + (1/2)C_{11,0}e_1^2 + (1/2)C_{33,0}e_3^2 + g_1e_1Q^2 + g_3e_3Q^2 \quad (17)$$

where  $g_1, g_3, h_1$  and  $h_3$  are the coupling constants. This expression of the free energy is discussed in [49], three temperatures are defined:  $T_0$  which is the transition equilibrium temperature,  $T_1$  and  $T_C$ .

$T_1$  is defined by  $\partial F/\partial Q = 0$  it gives  $T_1 = T_0 + b^2/(4ac)$ .

Above  $T_1$  the order parameter is zero ( $Q=0$ ).

In the temperature range  $T_0 < T < T_1$  the system is characterised by a stable state and a metastable state.

$T_C$  is defined by  $\partial F/\partial Q = 0$  and  $F=0$ , it results  $T_C = T_0 + 2b^2/(9ac)$

There is a discontinuous jump of the order parameter (first order) transition at  $T_C$ .

$$Q = \frac{b}{2c} + \sqrt{\frac{a}{c}}\sqrt{T_C - T} \quad (18)$$

In the temperature range  $T_0 < T < T_C$  the system has a stable state with  $Q \neq 0$  and a metastable state with  $Q=0$ . Finally below  $T_0$  the free energy has two minima both corresponding to  $Q \neq 0$

The occurrence of metastable states in the temperature range between  $T_0$  and  $T_1$  generates thermal hysteresis [49]. The difference between  $T_1$  and  $T_0$  gives an account for the hysteresis observed between heating and cooling. In the case of  $\text{Lu}_5\text{Ir}_4\text{Si}_{10}$  the phase transition occurs at  $T_0 = 80$  K on cooling and at  $T_1 = 81$  K on heating [34]. The thermal hysteresis  $\Delta T_{\text{hys}}$  is related to the coefficient  $b$  by the relation  $\Delta T_{\text{hys}} = T_1 - T_C \approx b^2/(4ac)$ . The small hysteresis  $\Delta T_{\text{hys}} \approx 1$  K implies that the cubic coefficient  $b$  is small compared to the quartic coefficient  $c$ . Using  $Q(0)^2 \approx (a/c)T_C$  from Equation (18) it results that  $\Delta T_{\text{hys}} \approx b^2T_C/(4c^2Q(0)^2)$ . Taking  $Q(0) \approx 1$  and  $T_C = 80$  K it gives  $b/c \approx 1/5$  for  $\text{Lu}_5\text{Ir}_4\text{Si}_{10}$ .

The first-order phase transition in  $\text{Lu}_5\text{Ir}_4\text{Si}_{10}$  is associated with a latent heat which is hard to detect and evaluate [30].

The specific heat in the low temperature phase transition is given by:

$$\frac{\Delta C_P}{V_m T} = \left\{ \frac{\partial S}{\partial T} \right\}_p = \frac{b}{4} [a/c]^{1.5} \frac{1}{\sqrt{(T_C - T)}} + \frac{a^2}{2c} \quad (19)$$

where  $V_m = 2 \times 10^{-4} \text{ m}^3$  is the molar volume. The first contribution of the specific heat follows a critical temperature dependence with the critical exponent  $-0.5$  which is responsible of the divergence of the specific heat at  $T_C$ . The second contribution to the specific heat corresponds to the value obtained at a second-order phase transition.

The new elastic stiffness components are

$$C_{11} \approx C_{11,0} - \frac{1}{2} \frac{g_1^2}{c} - \frac{g_1^2}{c} \frac{b}{\sqrt{ac}} \frac{1}{\sqrt{T_C - T}} \quad (20a)$$

$$C_{33} \approx C_{33,0} - \frac{1}{2} \frac{g_3^2}{c} - \frac{g_3^2}{c} \frac{b}{\sqrt{ac}} \frac{1}{\sqrt{T_C - T}} \quad (20b)$$

Combining the elastic data [34] with the specific heat results [30] (Table 1) allows us to determine all the coefficients of the free energy expansion for  $\text{Lu}_5\text{Ir}_4\text{Si}_{10}$ :  $a = 2 \times 10^5 \text{ J K}^{-1} \text{ m}^{-3}$ ,  $b = 3 \times 10^6 \text{ J m}^{-3}$ ,  $c = 2 \times 10^7 \text{ J m}^{-3}$ ,  $g_1 \approx g_3 \approx 9 \times 10^7 \text{ J m}^{-3}$ . These parameters are evaluated using  $Q(0) = 1$  at 0 K. An isotropic coupling constant with the components  $g_1 = g_2 \approx g_3$  is found in  $\text{Lu}_5\text{Ir}_4\text{Si}_{10}$  having a tetragonal symmetry. The values obtained for  $\text{TbTe}_3$  are the following:  $a = 8 \times 10^4 \text{ J K}^{-1} \text{ m}^{-3}$ ,  $c = 3 \times 10^7 \text{ J m}^{-3}$ ,  $g_1 \approx g_3 \approx 1 \times 10^8 \text{ J m}^{-3}$  and  $g_2 = 0$  calculated with the data taken from [26]. In contrast with  $\text{Lu}_5\text{Ir}_4\text{Si}_{10}$  a strong anisotropic coupling constant, whose components are  $g_1, g_2 = 0, g_3$ , characterises the (upper) CDW phase transitions in the two-dimensional rare earth tritellurides [23–28] and transition metal dichalcogenides compounds [16–21].

It is worth to note that the numerical values of the Landau coefficients  $a, c$  and the coupling constant  $g$  found in the materials  $\text{TbTe}_3$  and  $\text{Lu}_5\text{Ir}_4\text{Si}_{10}$  are very similar.

### 3. Discussion

In the following section, several materials will be discussed whose thermodynamic properties have been studied at the CDW phase transition.

The specific heat per unit volume jumps measured at the CDW (SDW) phase transition in several materials are reported in Table 1 and they are shown in Figure 5.

- (a) The quasi-one dimensional conductors  $\text{K}_{0.3}\text{MoO}_3$ ,  $\text{NbSe}_3$  and TTF-TCNQ exhibit a Peierls transition at 180, 145 and 55 K respectively. The thermodynamic properties have been studied in details [10–15]. The  $\text{K}_{0.3}\text{MoO}_3$  material is a model for the quasi-one-dimensional conductors.
- (b) An upper limit  $\Delta C_P \approx 0.5 \text{ J mol}^{-1} \text{ K}^{-1}$  has been estimated on the magnitude of any anomaly in the specific heat associated with the 30 K CDW transition in transition metal dichalcogenide  $2\text{H-NbSe}_2$  [16,17]
- (c) Specific heat jumps  $\Delta C_P \approx 1 \text{ J mol}^{-1} \text{ K}^{-1}$  in  $\text{ErTe}_3$  and  $\Delta C_P \approx 3 \text{ J mol}^{-1} \text{ K}^{-1}$  in  $\text{TbTe}_3$  are observed at the upper CDW phase transition  $T_{\text{CDW1}}$  respectively 330 and 260 K [26,27]. A specific heat jump  $\Delta C_P \approx 0.5 \text{ J mol}^{-1} \text{ K}^{-1}$  is observed at the lower CDW transition  $T_{\text{CDW2}}$  (150 K) in  $\text{ErTe}_3$ .
- (d) The first-order phase transition observed in  $\text{Lu}_5\text{Ir}_4\text{Si}_{10}$  is characterised by a large specific heat jump, changes in the thermal expansion coefficients, and a sudden drop of the electric resistivity [29–33].

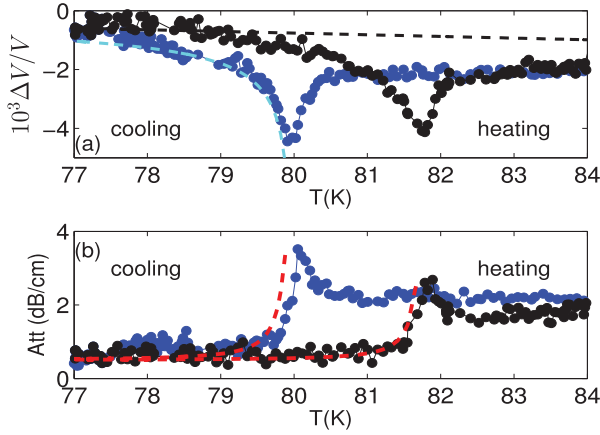


**Figure 5.** (a) Velocity decrease ( $V_{11}$ ) of the longitudinal  $C_{11}$  mode at the CDW phase transition in  $\text{Lu}_5\text{Ir}_4\text{Si}_{10}$ . The dotted cyan curve is calculated using  $\Delta V/V = 2 \times 10^{-4} \{(80 - T)/80\}^{-1}$  (cooling). (b) Attenuation of the  $C_{11}$  mode. The dashed red curves are calculated using  $\text{Att} = 10\omega\tau_{\text{LK}}/(1 + (\omega\tau_{\text{LK}})^2)$  with  $\tau_{\text{LK}} = 1.1 \times 10^{-11} \{(80 - T)/80\}^{-1}$  (s) (cooling),  $\tau_{\text{LK}} = 1.1 \times 10^{-11} \{(81.8 - T)/81.8\}^{-1}$  (s) (heating) at frequency  $\omega/2\pi = 15$  MHz, temperature sweep rate 0.1 K/min, data taken from [34]. (Colour online)

A CDW is observed in  $\text{LaAgSb}_2$  at 210 K [35], but no elastic constant measurements are reported in this material.

- (e) The oxyborate  $\text{Fe}_3\text{O}_2\text{BO}_3$  presents a charge density wave transition at 290 K which is associated with a well defined anomaly in the specific heat reported in Figure 2 of [36]. Mössbauer spectroscopic studies are reported in [37]
- (f) In the case of spin density waves in antiferromagnetic Cr, a specific heat jump [38] and a decrease in the elastic constant  $C_{11}$  [39] observed at the SDW phase temperature  $T_N = 310$  K. They are in agreement with the mean field theory and the results satisfy the relations of Ehrenfest type [38].

The experimental data obtained with the CDW systems  $\text{K}_{0.3}\text{MoO}_3$ , TTF-TCNQ,  $2\text{H-NbSe}_2$ ,  $\text{TbTe}_3$  and  $\text{ErTe}_3$  can be described reasonably by the BCS lineal dependence Equation (10) (red dotted line in Figure 5) and described by:

$$\Delta C_P/V_m = AT_{\text{CDW}} \quad (21a)$$

$$A \approx 10N_0N(E_F)k_B^2 \quad (21b)$$

where  $N(E_F)$  is the density of states and  $N_0$  is the Avogadro number. The value  $A = 200 \text{ J K}^{-2} \text{ m}^{-3}$  gives a density of state  $N(E_F) \approx 2$  states/eV/unit cell for  $\text{TbTe}_3$  which is similar to the value  $N(E_F) = 1.5$  states/eV/unit cell reported in [24] (Table 2). A similar value of the density of states is found for the compounds  $\text{K}_{0.3}\text{MoO}_3$ ,  $\text{NbSe}_3$ . A larger value of about 7 states/eV/unit cell is deduced for TTF-TCNQ. The specific heat jump measured with  $2\text{H-TaSe}_2$  do not follow the BCS behaviour (Equation (21b)) as explained by McMillan

[42–44] who reformulated the theory, assuming that the coherence length is very short and that the dominant entropy is the lattice entropy. A pseudogap in the density of states of the electronic states was introduced in the microscopic theory of the quasi-one-dimensional materials [46]. TiSe<sub>2</sub> has received significant research attentions but the microscopic model is still unknown, an excitonic insulator state has been proposed to explain the charge ordering in this compound [9]. A weak first-order Néel transition is observed in chromium below at  $T_N \approx 312$  K is due to a spin density wave (SDW) in the conduction electron gas [38–41]. A survey of the properties of chromium is given by Fawcett [41]. The richness of the phenomena observed in Cr derives from its itinerant spin-density-wave antiferromagnet and many theoretical and experimental studies have been reported. A phenomenological model based on a mean field was proposed by Walter and [40,41]. The Landau free energy of the system is expanded in powers of the components of the SDW polarisation (linear or helical) vector. The small molar volume of Cr yields that the discontinuity in the specific heat per unit volume at  $T_N$  is ten times larger than the value given by Equation (21a).

The intermetallic compound Lu<sub>5</sub>Ir<sub>4</sub>Si<sub>10</sub> exhibits a first order structural phase transition with a divergence of the specific heat anomaly.

### 3.1. Elastic constant anomaly at the CDW phase transition

The rare earth tritellurides  $R\text{Te}_3$  crystallise in a weakly orthorhombic structure with the in-plane crystallographic  $\vec{a}$  and  $\vec{c}$  axes and lattice consists of stacked Te layers alternating with RTe layers. In contrast Lu<sub>5</sub>Ir<sub>4</sub>Si<sub>10</sub> has a tetragonal-symmetry system (crystallographic axes  $\vec{a} = \vec{b}$  and  $\vec{c}$ ). The longitudinal modes  $C_{11}$  and  $C_{33}$  propagate along the crystallographic  $\vec{a}$  and  $\vec{c}$  axes respectively at a velocity  $V_{11} = \sqrt{\frac{C_{11}}{\rho}}$  and  $V_{33} = \sqrt{\frac{C_{33}}{\rho}}$ , respectively, and  $\rho$  is the mass density. The discontinuities  $\Delta V_{ii}/V_{ii}$  ( $i=1$  and  $3$ ) of the velocity of the longitudinal modes measured at the CDW (SDW) phase transition are shown in Figure 6.

A small discontinuity of velocity  $\Delta V_{11}/V_{11} \approx 0.0005$  in the longitudinal  $C_{11}$  mode propagating in the basal plane is found at the low phase transition temperature 30 K transition in 2H-NbSe<sub>2</sub> [16]. In contrast a large discontinuity ( $\Delta V_{11}/V_{11} = 0.05$ ) of the velocity of the elastic constant  $C_{11}$  of TiSe<sub>2</sub> is measured at the high phase transition temperature  $T_{\text{CDW}} = 200$  K [18]. A large decrease of the velocities  $\Delta V_{11}/V_{11} \approx 0.01$  and  $\Delta V_{33}/V_{33} \approx 0.01$  of the longitudinal  $C_{11}$  and  $C_{33}$  modes is observed at the upper CDW phase transitions in ErTe<sub>3</sub> and TbTe<sub>3</sub> [26,27]. In contrast, a small decrease  $\Delta V_{33}/V_{33} \approx 0.002$  of the longitudinal  $C_{33}$  mode is observed at the lower CDW phase transitions  $T_{\text{CDW}2}$  150 and 120 K in ErTe<sub>3</sub> and HoTe<sub>3</sub> respectively.

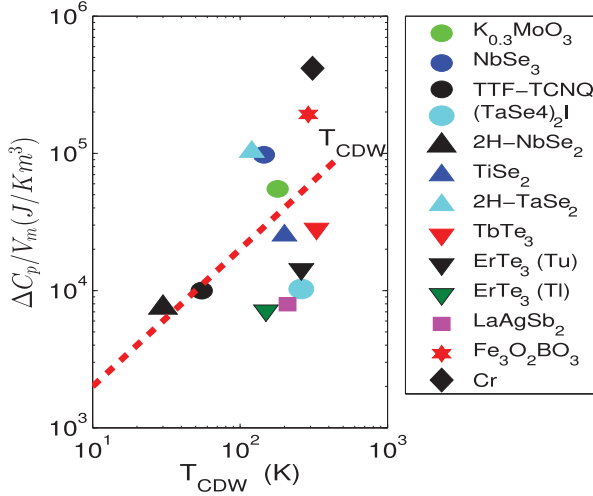


**Figure 6.** Specific heat jumps at the CDW and SDW phase transition in several materials as a function of  $T_{CDW}$  ( $T_{CDW}$ ) (Table 1); Tu means upper CDW Phase transition temperature  $T_{CDW1} = 260$  K (ErTe<sub>3</sub>) and Tl means lower CDW phase transition temperature  $T_{CDW2} = 150$  K (ErTe<sub>3</sub>). The red dashed line is calculated using  $\Delta C_p/V_m = AT_{CDW}^2$  with  $A = 200 \text{ JK}^{-2} \text{ m}^{-3}$ . (Colour online)

A remarkable feature is that many experimental data  $\Delta V_{ii}/V_{ii}$  with  $i=1$  and  $3$  follow approximately a  $T_{CDW}^2$  dependence (black dashed line) in Figure 6 given by:

$$\Delta V_{ii}/V_{ii} = BT_{CDW}^2 \quad (22)$$

$B = 4 \times 10^{-7} \text{ K}^{-2}$ . This temperature dependence is approximately verified by most of the materials such as quasi one dimensional conductor  $K_{0.3}MoO_3$ , transition metal dichalcogenide 2H-NbSe<sub>2</sub> and rare earth tritellurides TbTe<sub>3</sub>, ErTe<sub>3</sub> and HoTe<sub>3</sub> at the upper and lower CDW phase transitions and Cr. They are characterised by the same coefficient B (Equation (22)) related to the longitudinal mode  $C_{33}$  or  $C_{11}$  in the Landau approach. Such a quadratic behaviour of  $\Delta V_{ii}/V_{ii}$  ( $i=1$  and  $3$ ) in Equation (22) is expected from the Ehrenfest relation (Equation (15)). Similar experimental value of the stress derivative of the logarithmic of the transition temperature  $d(\ln(T_{CDW})/d\sigma) \approx 0.3$  and  $0.8 \text{ GPa}^{-1}$  is found in rare earth tritellurides TbTe<sub>3</sub> [26] and 2H-NbSe<sub>2</sub> [16].

The discontinuities  $\Delta V_{11}/V_{11} \approx 0.005$  and  $\Delta V_{33}/V_{33} \approx 0.005$  in the velocities of the longitudinal  $C_{11}$  and  $C_{33}$  modes found at the first-order structural phase transition at 80 K in Lu<sub>5</sub>Ir<sub>4</sub>Si<sub>10</sub> [34] are situated on the black dotted line described by Equation (25). But a first-order transition is observed in the case of Lu<sub>5</sub>Ir<sub>4</sub>Si<sub>10</sub>.

In contrast 2H-TaSe<sub>2</sub>, (TaSe<sub>4</sub>)<sub>2</sub>I, and NbSe<sub>3</sub> do not follow Equation (25) (black dotted line Figure 6).

The coupling constants  $g'_1$  and  $g'_3$  can be deduced from the experimental-specific heat jumps  $\Delta C_P$  and the velocity decreases  $\Delta V_{11}/V_{11}$  and  $\Delta V_{33}/V_{33}$  using Equation (13a) and Equation (13b) (the order parameter being the energy gap [45]) which gives:

$$g_1'^2 \approx \frac{\Delta C_P}{V_m} \frac{\Delta V_{11}}{V_{11}} \frac{C_{11}}{100k_B^4 T_{CDW}^3 N_0} \quad (23a)$$

$$g_3'^2 \approx \frac{\Delta C_P}{V_m} \frac{\Delta V_{33}}{V_{33}} \frac{C_{33}}{100k_B^4 T_{CDW}^3 N_0} \quad (23b)$$

In order to compare the value of the coupling constant of the rare earth tritellurides with those of the transition metal dichalcogenides where a 3 state CDW state is found, we take the factor of 3 into account [42–44]. Furthermore a larger value of the elastic stiffness components  $C_{11}$  or  $C_{33}$  of 100 GPa is used in Equation (23a) or Equation (23b) for  $TbTe_3$  and  $ErTe_3$  in contrast to the smaller value 50 GP reported in Table 1. The values of  $g'_1$  and  $g'_3$  are now given in  $eV^{-1} m^{-3}$  and they are reported in Figure 7. A mean coupling coefficient value  $\approx 0.08 eV^{-1} m^{-3}$  is obtained for the quasi-one conductors TTF-TCNQ and  $K_{0.3}MoO_3$  and transition metal dichalcogenides 2H-NbSe<sub>2</sub> and TiSe<sub>2</sub>. For these materials large values of the Young modulus  $Y \approx 100$  GPa are reported (Table 1)

Similar values  $g'_1 \approx g'_3 \approx 0.04 eV^{-1} m^{-3}$  are found at the upper CDW phase transition respectively in the rare earth tritellurides  $TbTe_3$  and  $ErTe_3$ . Such a coupling constant  $g'_1(g'_3)$  is related to the atomic displacements in the square Te sheets associated to the CDW phase transition [22–24]. The

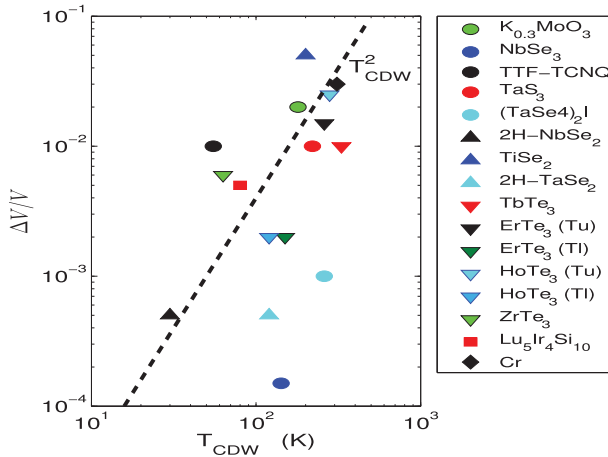


**Figure 7.** Velocity discontinuities (indexes are not indicated) at the CDW and SDW phase transitions in several materials as a function of  $T_{CDW}$  ( $T_{SDW}$ ) (Table 1). Tu means upper CDW Phase transition temperature  $T_{CDW1} = 260$  K ( $ErTe_3$ ) and Tl means lower CDW phase transition temperature  $T_{CDW2} = 150$  K ( $ErTe_3$ ). The black dashed line is calculated using  $\Delta V/V = BT_{CDW}^2$  with  $B = 4 \times 10^{-7} K^{-2}$ . (Colour online)



incommensurate lattice modulation has a unidirectional wavevector  $q_1 = (2/7)c^*$  ( $c^* = 2\pi/c$ ). The crystallographic  $\vec{b}$  is perpendicular to the Te planes. No atomic displacement along  $\vec{b}$  is in agreement with the component  $g_2 = 0$  observed at the upper CDW transition in  $\text{TbTe}_3$ ,  $\text{ErTe}_3$  and  $\text{HoTe}_3$ . Small dips in the velocity ( $\Delta V_{ii}/V_{ii} \approx 0.002$ ,  $i=1$  and  $3$ ) are detected for the longitudinal  $C_{11}$  and  $C_{33}$  modes at the lower CDW phase transition ( $T_{\text{CDW}2}$ ) in  $\text{ErTe}_3$  and  $\text{HoTe}_3$  (Table 1) having a wavevector  $q_2 = (1/3)a^*$  ( $a^* = 2\pi/a$ ) perpendicular to the first wavevector  $q_1$ . A slightly smaller coupling constant is obtained for this transition:  $g'_1 \approx g'_3 \approx 0.03 \text{ eV}^{-1} \text{ m}^{-3}$ . Anisotropy of the coupling constant is related to the uniaxial lattice distortion which accompanies the CDW phase transition.

In contrast the acoustic anomaly in Cr is quantitatively more pronounced which is reflected by the larger value of the order parameter coupling whose magnitude is found to be  $g'_3 \approx 0.3 \text{ eV}^{-1} \text{ m}^{-3}$  (Figure 7).

We have presented an analysis of the anomalies of the longitudinal elastic constants of several materials in the vicinity of the CDW phase transition (normal-incommensurate second-order phase transition). The analysis has been performed in the framework of the mean field theory and using the Allender et al. model [45].

### 3.2. Dynamic behaviour

Only static effects of the order parameter have been considered above. The sound velocity is primarily determined by the static properties of the order parameter. The attenuation and part of the velocity behaviour are connected with the dynamics of the order parameter [10,51–54]. Some features of the sound velocity and especially the ultrasonic attenuation depend on the dynamic behaviour of the order parameter. The fluctuations of the order parameter near the second-order phase transition leads to a decrease of the sound velocity and an increase in the attenuation coefficient. Many studies of the dynamics in incommensurate phases have been reported as in [53,54]. The characteristic feature of incommensurate structure is the presence of two branches in its vibrational spectrum: Amplitude and Phase modes (amplitudon and phason). The phason branch has no gap and the amplitudon is similar to a soft mode [55]. The interaction terms between the acoustic waves and the amplitude and phase modes have been derived by Bruce and Cowley [55]. The interactions with the amplitude mode affects the velocity of the acoustic wave but not the interactions with the phase mode. Dynamic behaviour is usually discussed in terms of two distinct mechanisms [54]: relaxation behaviour and fluctuation behaviour. The first term called Landau-Khalatnikov term is related to the relaxation of the order parameter which takes place in the ordered phase. The influence of amplitude mode has been frequently considered in the incommensurate phase transitions [54]. The relaxation behaviour is characterised by

the relaxation time  $\tau_{LK}$  with  $\tau_{LK} = \tau_{LK}^0(1 - T/T_{CDW})^{-1}$  and  $\tau_{LK}$  is infinite at  $T_{CDW}$  [53]. The amplitude mode is similar to a soft mode,  $\omega_A = 0$  at the phase transition  $T_{CDW}$ . Velocity and attenuation are expressed as a function of the measurement angular frequency  $\omega$  and  $\tau_{LK}$  by

$$\left\{ \frac{\Delta V}{V} \right\}_{LK} = \left\{ \frac{\Delta V}{V} \right\}_{LK,0} \frac{\omega^2 \tau_{LK}^2}{1 + \omega^2 \tau_{LK}^2} \quad (24)$$

$$Att_{LK} = \left\{ \frac{\Delta V}{V^2} \right\}_0 \frac{\omega^2 \tau_{LK}}{1 + \omega^2 \tau_{LK}^2} \quad (25)$$

The indexes are not indicated in this section. The temperature dependence of the attenuation just below  $T_{CDW}$  is described by a small time constant  $\tau_{LK}^0 \approx 2 \times 10^{-12}$  s observed for  $TbTe_3$  (Figure 2). A slightly larger time constant  $\tau_{LK}^0 \approx 1 \times 10^{-11}$  s is found for  $ErTe_3$ ,  $HoTe_3$  and  $Lu_5Ir_4Si_{10}$  (Figures 3 and 8, Table 3).

Many aspects of the Landau-Khalatnikov behaviour of the elastic velocity and attenuation of the longitudinal  $C_{11}$  and  $C_{33}$  near the incommensurate CDW transition in  $RTe_3$  are similar to those found at the normal-incommensurate structural transition such as  $K_2SeO_4$  and  $Rb_2ZnCl_4$  [51–54]. The values of the relaxation times related to the Landau Khalatnikov behaviour  $\tau_{LK}$  are very close (Table 3). Nevertheless, the amplitudes of the anomalies in attenuation observed in rare earth tritellurides are smaller. But the physical mechanisms which drive the transition in insulators and conductors are different. In conductors, the incommensurate structure arise from the interaction between conduction electrons and the atomic lattice (Peierls mechanism) [1,56]. Coulomb and short range forces exist in insulators and the displacive transition has a lattice-dynamical origin [57].

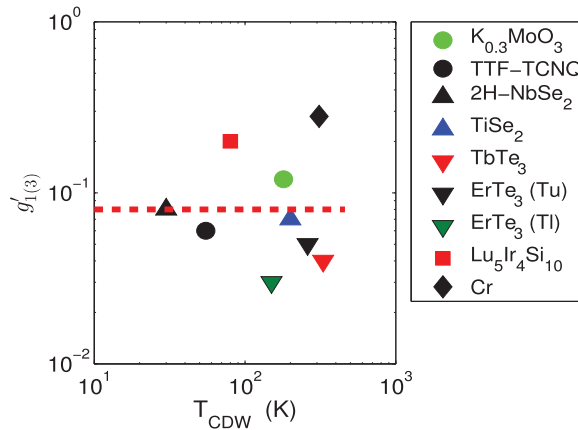


**Figure 8.** Coupling coefficients  $g'_1$  or  $g'_3$ , Tu means upper CDW phase transition temperature  $T_{CDW1} = 260$  K ( $ErTe_3$ ) and TI means lower CDW phase transition temperature  $T_{CDW2} = 150$  K ( $ErTe_3$ ). (Colour online)

**Table 3.** Dynamic behaviours, critical exponents  $\mu$ ,  $z\nu$ , relaxation times  $\tau_{LK}^0$  and  $\tau_F^0$ .

Materials		
TbTe <sub>3</sub>	$\mu = -0.026, z\nu = 1.36$	$\tau_{LK}^0 = 2 \times 10^{-12}$ (s) $\tau_F^0 \approx 1 \times 10^{-11}$ (s)
ErTe <sub>3</sub>	$\mu = -0.026, z\nu = 1.36$	$\tau_{LK}^0 = 5 \times 10^{-11}$ (s) $\tau_F^0 \approx 1 \times 10^{-11}$ (s)
HoTe <sub>3</sub>	$\mu = -0.026, z\nu = 1.36$	$\tau_{LK}^0 = 2 \times 10^{-11}$ (s) $\tau_F^0 \approx 3 \times 10^{-11}$ (s)
Lu <sub>5</sub> Ir <sub>4</sub> Si <sub>10</sub>	$\mu = 0.5, 0.2, z\nu \approx 1$	$\tau_{LK}^0 = 1.1 \times 10^{-11}$ (s) $\tau_F^0 \approx 1 \times 10^{-11}$ (s)

The second contribution is related to fluctuations and it is not easy to separate both contributions at temperatures below the phase transition [54]. For this reason, the fluctuation behaviour is considered only at temperatures above the phase transition and is characterised by the relaxation time  $\tau_F$  defined by  $\tau_F = \tau_F^0 (T/T_C - 1)^{z\nu}$  where  $z$  is the critical dynamic exponent defined by  $\tau_F = \xi^z$  and  $\xi = \xi_0^{-\nu}$  is the correlation length.

The fluctuation contributions to the velocity  $V$  and attenuation are described by the following phenomenological forms [51–54]:

$$\left\{ \frac{\Delta V}{V} \right\}_F \approx t^{-\mu}; \quad \text{Att}_F \approx \omega^2 t^{-\mu-z\nu} \quad (26)$$

The incommensurate systems have been discussed by Cowley and Bruce [55] who predict that the critical behaviour near phase transition should conform to 3D-XY universality. The fluctuation contributions have the critical exponents  $\mu = -0.026$  and  $z\nu = 1.36$ . They are described by functions of the form [53]:

$$\left\{ \frac{\Delta V}{V} \right\}_F = C - Dt^{0.026} \quad (27)$$

$$\text{Att}_F = \left\{ \frac{C - Dt^{0.026}}{V} \right\} \omega^2 \tau_F \quad (28)$$

where the reduced temperature is  $t = (T - T_{CDW})/T_{CDW}$  and  $C$  and  $D$  are adjustable parameters,  $\omega$  is the measurement angular wave frequency.

The critical behaviours observed with the quasi-one-dimensional conductor  $K_{0.3}\text{MoO}_3$  [10] and the rare earth tritellurides TbTe<sub>3</sub>, ErTe<sub>3</sub> and HoTe<sub>3</sub> (Figures 2–4, 8 and 9) are in agreement with the 3D-XY model characterised by the critical exponents 0.026 and  $z\nu = 1.36$  [26–28].

In contrast, the critical exponent ( $\mu = 0.5$ ) observed for Lu<sub>5</sub>Ir<sub>4</sub>Si<sub>10</sub> in Figures 8 and 10 in the ordered phase is in agreement with (Equation (20a)). A smaller exponent  $\mu = 0.2$  is found in the disordered high-temperature phase (Figure 10).

Attenuation behaviour can be described by the critical exponent  $z\nu = 1$  (Figure 10).

In summary, near the normal-incommensurate CDW phase transition [54], two dynamic regimes are defined: As temperature approaches  $T_{CDW}$ , the relaxation time  $\tau_F$  increases and governs the temperature behaviour of velocity and

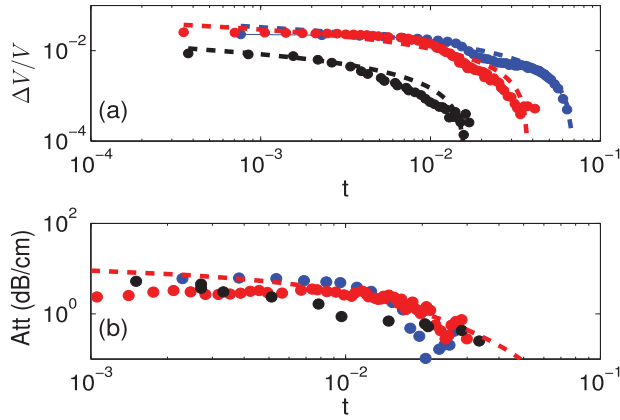


**Figure 9.** (a) Critical velocity contributions  $\delta V_{11}/V_{11}$  of the  $C_{11}$  mode in ErTe<sub>3</sub> (blue symbols) and HoTe<sub>3</sub> (red symbols) and  $C_{33}$  mode TbTe<sub>3</sub> (black symbols). The dashed curves are calculated curves with 3D XY model,  $\delta V_{11}/V_{11} = 0.319 - 0.342 \times t^{0.026}$  for ErTe<sub>3</sub>,  $\delta V_{33}/V_{33} = 0.12 - 0.1336 \times t^{0.026}$  for TbTe<sub>3</sub> and  $\delta V_{33}/V_{33} = 0.326 - 0.355 \times t^{0.026}$  for HoTe<sub>3</sub>.  $t$  is the reduced temperature  $t = (T - T_{CDW})/T_{CDW}$ . (b) Critical attenuation (same symbols). The dashed red curve is calculated using Equation (27) (3D XY model) with the relaxation time  $\tau_F^0 = 1 \times 10^{-11}$  s, data taken from [26–28]. (Colour online)

attenuation. Below  $T_{CDW}$  Landau-Khalatnikov (order parameter) relaxation contributes to attenuation.

#### 4. Conclusion

Properties of rare earth tritellurides  $R\text{Te}_3$  and  $\text{Lu}_5\text{Ir}_4\text{Si}_{10}$  compounds at the CDW phase transition are briefly discussed in the framework of mean field

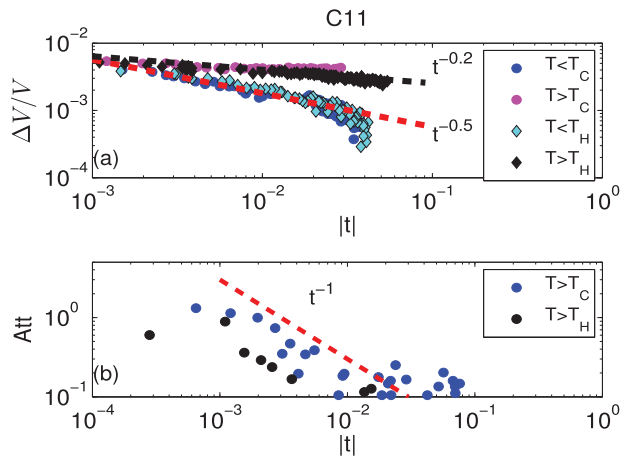


**Figure 10.** (a) Critical velocity contributions  $\delta V_{11}/V_{11}$  of the  $C_{11}$  mode in  $\text{Lu}_5\text{Ir}_4\text{Si}_{10}$ . The dashed red lines are calculated using  $\delta V_{11}/V_{11} = 6 \times 10^{-4} t^{-0.5}$  and  $\delta V_{11}/V_{11} = 2 \times 10^{-4} t^{-0.2}$ . (b) Critical attenuation, the dashed red line represents  $t^{-1}$  variation,  $t$  is the reduced temperature  $t = |T - T_C|/T_C$  or  $t = |T - T_H|/T_H$ , data taken from [34]. (Colour online)

theory. Attenuation and longitudinal velocity changes near  $T_{\text{CDW}}$  are briefly reviewed. It is interesting to compare the results with and without the effects of fluctuations. Similar features in the thermodynamic properties at the CDW phase transition are found in the following compounds: The quasi-one conductors TTF-TCNQ and  $\text{K}_{0.3}\text{MoO}_3$ , the transition metal dichalcogenide  $2\text{H-NbSe}_2$  and the rare earth tritellurides  $\text{TbTe}_3$ ,  $\text{ErTe}_3$ ,  $\text{HoTe}_3$ . It appears that the amplitude of the specific heat jump at the CDW phase transition increases linearly with increasing  $T_{\text{CDW}}$ . The same dependence  $\Delta C_P/V_m = AT_{\text{CDW}}$  ( $A = 200 \text{ JK}^{-2} \text{ m}^{-3}$ ) is found. In the same manner, the amplitude of the discontinuity of the velocity of the longitudinal elastic constants increases with increasing  $T_{\text{CDW}}$  is observed for the same materials as  $\Delta V_{ii}/V_{ii} = BT_{\text{CDW}}^2$  ( $i=1$  and  $3$  and  $B = 4 \times 10^{-7} \text{ K}^{-2}$ ). Such a quadratic dependence is in agreement with the BCS theory (Allender et al. model) and the Ehrenfest relationships. It results that the thermodynamic properties of  $2\text{H-NbSe}_2$ , TTF-TCNQ,  $\text{K}_{0.3}\text{MoO}_3$ ,  $\text{TbTe}_3$ ,  $\text{ErTe}_3$  and  $\text{HoTe}_3$  have the same behaviour and they follow approximately the classical mean field BCS type behaviour. Nevertheless, this simple approach fails to describe adequately the specific heat and elastic stiffness properties of all CDW systems in particular the transition metal dichalcogenides. Discrepancies are attributed to the different contributions given by fluctuations and the amplitude mode at the incommensurate CDW phase transition which are sample dependent. The characteristic time governing the order parameter dynamics increases critically toward the transition  $\tau_{\text{LK}} = \tau_{\text{LK}}^0(1 - T/T_{\text{CDW}})^{-1}$ , a relaxation time  $\tau_{\text{LK}}^0 \approx 1 \times 10^{-11} \text{ s}$  is found for the rare earth tritelluride compounds  $\text{TbTe}_3$ ,  $\text{ErTe}_3$  and  $\text{HoTe}_3$  and the intermetallic compound  $\text{Lu}_5\text{Ir}_4\text{Si}_{10}$ . The transition which occurs in the compound  $\text{Lu}_5\text{Ir}_4\text{Si}_{10}$  is first order and can be described by the Landau theory including a cubic term in the expansion of the free energy.

## Disclosure statement

No potential conflict of interest was reported by the author(s).

## References

- [1] G. Grüner, *Density Waves in Solids*, Addison-Wesley, Boston, MA, 1994.
- [2] H. Frölich, *Basic Number Theory*, Proceedings of the Royal Society, London, 1954.
- [3] J.W. Brill, in *Elastic Properties of Low Dimensional Materials*, M. Levy, Bass and Stern, eds., Academic Press, London, 2001.
- [4] P. Monceau, *Electronics crystals: An experimental overview*, Adv. Phys. 61 (2012), pp. 325–581.
- [5] M.D. Johannes and I. Mazin, *Fermi surface nesting and the origin of Charge Density Wave in metals*, Phy. Rev. B 77 (2008), p. 165135.

- [6] X. Zhu, J. Guo, J. Zhang, E.W. Plummer, and J.D. Guo, *Classification of charge density waves based on their nature*, Proc. Natl. Acad. Sci. 112 (2015), pp. 2367–2371. doi:10.1073/pnas.1424791112
- [7] X. Zhu, J. Guo, J. Zhang, E.W. Plummer, and J.D. Guo, *Misconception associated with the origin of charge density waves*, Adv. Phys. 2 (2017), pp. 622–640. doi:10.1080/23746149.2017.1343098
- [8] C.-H. Chen, J. Choe, and E. Morosa, *Charge density wave in strongly correlated electron systems*, Rep. Prog. Phys. 79 (2016), pp. 16428–16442.
- [9] K. Rossnagel, *On the origin of charge density waves in selected layered transition metal dichalcogenides*, J. Phys. Condens. Matter. 23 (2011), p. 213001.
- [10] J.W. Brill, M. Chung, Y.-K. Kuo, E. Figueroa, and G. Mozurkewich, *Thermodynamic of the charge density wave transition in blue bronze*, Phys. Rev. Lett. 74 (1995), pp. 1182–1185. doi:10.1103/PhysRevLett.74.1182
- [11] J.A. Aronovitz, P. Goldart, and G. Mozurkewich, *Elastic singularities at the peierls transition*, Phys. Rev. Lett. 64 (1990), pp. 2799–2802. doi:10.1103/PhysRevLett.64.2799
- [12] S. Tomic, K. Biljakovic, D. Djurek, J.R. Cooper, P. Monceau, and A. Meershaut, *Calorimetry study of the phase transition in NbSe<sub>3</sub>*, Solid State Commun. 38 (1981), pp. 109–112.
- [13] R.A. Craven, M.B. Salamon, G. DePasquali, R.M. Herman, G. Stucky, and A. Schultz, *Specific heat OF tetrathiofulvanium-Tetracyanoquinodimethane(TTF-TCNQ) in the vicinity of the metal-insulator transition*, Phys. Rev. Lett. 32 (1974), pp. 769–772. doi:10.1103/PhysRevLett.32.769
- [14] M. Barmatz, L.R. Testardi, A.F. Garito, and A.J. Heeger, *Temperature dependence of sound velocities in TTF-TCNQ*, Solid State Commun. 15 (1974), pp. 1299–1302. doi:10.1016/0038-1098(74)91366-0
- [15] J.W. Brill and N.P. Ong, *Young's modulus of NbSe<sub>3</sub>*, Solid State Commun. 25 (1978), pp. 1075–1078. doi:10.106/0038-1098(78)90910-9
- [16] V. Ermenko, V. Sirenko, V. Ibilayev, B. Bartolome, A. Arauzo, and G. Reményi, *Heat capacity, thermal expansion, and pressure derivative of critical temperature at the superconducting and charge density wave in NbSe<sub>2</sub>*, Physica C 469 (2009), pp. 259–264. doi:10.1016/j.physc.2009.02.015
- [17] M.H. Jericho, A.M. Simpson, and R.F. Frindt, *Velocity of ultrasonic waves in 2H – NbSe<sub>2</sub>, 2H – TaSe<sub>2</sub>, 1T – TaS<sub>2</sub>*, Phys. Rev. B 22 (1980), pp. 4907–4914. doi:10.1103/PhysRevB.22.4907
- [18] M. Barmatz, L.R. Testardi, and F.J. DiSalvo, *Elastic measurements in the layered NbSe<sub>2</sub>*, Phys. Rev. B 12 (1975), pp. 4367–4376. doi:10.1103/PhysRevB.12.4367
- [19] R.A. Craven and S.F. Meyer, *Specific heat and resistivity near the charge density wave transition in 2H – TaSe<sub>2</sub> and 2H – TaS<sub>2</sub>*, Phys. Rev. B 16 (1977), pp. 4583–4593. doi:10.1103/PhysRevB.16.4583
- [20] A. Caillé, Y. Lepine, M.H. Jericho, and A.M. Simpson, *Thermal expansion ultrasonic velocity and attenuation measurements in TiSe<sub>2</sub>, TiS<sub>2</sub> and TiS<sub>0.5</sub>Se<sub>1.5</sub>*, Phys. Rev. B 28 (1983), pp. 5454–5461, pp. 4583–4593. doi:10.1103/PhysRevB.28.5454
- [21] R.A. Craven, F. DiSalvo, and F.S. Hsu, *Mechanism for the 200 K transition in TiSe<sub>2</sub>: A measurement of the specific heat*, Solid State Commun. 25 (1978), pp. 39–42. doi:10.1016/0038-1098(78)91165-1
- [22] E. DiMasi, M.C. Arosón, J.F. Mansfield, B. Foran, and S. Lee, *Effects of chemical pressure and charge density waves transition in rare earth tritellurides*, Phys. Rev. B 52 (1995), pp. 14516–14525. doi:10.1103/PhysRevB.52.14516

- [23] N. Ru, C.L. Condon, G.Y. Margulis, K.Y. Shin, J. Laverock, S.B. Dugdale, M.F. Toney, and I.R. Fisher, *Effects of chemical pressure on the charge density wave transition in rare earth tritellurides*, Phys. Rev. B 77 (2008), p. 035114. doi:10.1103/PhysRevB.77.035114
- [24] V. Brouet, W.L. Yang, X.J. Zhou, Z. Hussain, R.G. Moore, R. He, D.H. Lu, Z.X. Shen, J. Laverock, S.B. Dugdale, and I.R. Fisher, *Angle resolved photoemission study of the evolution of band structure and charge density wave in  $R\text{Te}_3$  ( $R = \text{Y, La, Ce, Tb, and Dy}$ )*, Phys. Rev. B 77 (2008), p. 433. doi:10.1103/PhysRevB.77.235104
- [25] M. Maschek, S. Rosenkranz, A.H. Said, P. Giraldo-Gallo, I.R. Fisher, and F. Weber, *Wave-vector-dependent electron phonon coupling and the charge density wave transition in  $\text{TbTe}_3$* , Phys. Rev. B 91 (2015), p. 235146. doi:10.1103/PhysRevB.91.235146
- [26] M. Saint-Paul, C. Guttin, P. Lejay, G. Reményi, and P. Monceau, *Elastic anomalies at the charge density wave system  $\text{TbTe}_3$* , Solid State Commun. 233 (2016), pp. 24–29. doi:10.1016/j.ssc.2016.02.008
- [27] M. Saint-Paul, C. Guttin, P. Lejay, G. Reményi, and P. Monceau, *Elastic anomalies and critical properties at the charge density wave system  $\text{ErTe}_3$* , Physica B 504 (2017), pp. 39–46. doi:10.1016/j.physb.2016.10.009
- [28] M. Saint-Paul, C. Guttin, P. Lejay, O. Leynaud, and P. Monceau, *Elastic anomalies at the charge density wave system  $\text{HoTe}_3$* , Int. J. Modern Phys. B 32 (2018), p. 52018. doi:10.1142/S0217979218502491
- [29] S. VanSmaalen, M. Shaez, L. Palatinus, P. Daniels, F. Galli, G.J. Nieuwenhuys, and J.A. Mydosh, *Multiple density waves in  $R5\text{Ir}_4\text{Si}_10$* , Phys. Rev. B 69 (2004), p. 014103. doi:10.1103/PhysRevB.69.014103
- [30] Y.-K. Kuo, C.S. Lue, F.H. Hsu, H.H. Lu, H.D. Yang, and M.S. Anderson, *Thermal properties of  $\text{Lu}_5\text{Ir}_4\text{Si}_{10}$  near the charge density wave transition*, Phys. Rev. B 64 (2001), p. 124124. doi:10.1103/PhysRevB.64.125124
- [31] R.N. Shelton, L.S. Haussermann-Berg, P. Klavins, H.D. Yang, M.S. Anderson, and C.A. Swenson, *Electronic phase transition and partially gapped fermi surface in superconducting  $\text{Lu}_5\text{Ir}_4\text{Si}_{10}$* , Phys. Rev. B 34 (1986), pp. 4590–4594. doi:10.1103/PhysRevB.34.4590
- [32] B. Mansart, M.J.G. Cottet, T.J. Penfold, S.B. Dugdale, R. Tediosi, M. Chergui, and F. Carbone, *Evidence for a peierls phase transition in a three-dimensional multiple charge density wave in solids*, Proc. Natl. Acad. Sci. 109 (2012), pp. 5603–5608. doi:10.1073/pnas.1117028109
- [33] S. Ramakrishnan and S. van Smaalen, *Evidence for a peierls phase transition in a three-Dimensional multiple charge density wave in solids*, Rep. Prog. Phys. 80 (2017), p. 116501. doi:10.1088/1361-6633/aa7d5f
- [34] M. Saint-Paul, C. Opagiste, and C. Guttin, *Elastic properties at the first order transition in  $\text{Lu}_5\text{Ir}_4\text{Si}_{10}$* , J. Phys. Chem. Solids 138 (2020), p. 109255. doi:10.1016/j.pcs.2019.109255
- [35] S.L. Bud'ko, S.A. Law, P.C. Canfield, G.D. Samolyuk, M.S. Torikachvili, and G.M. Schmiedeshoff, *Thermal expansion and magnetostriction of pure and doped  $\text{RAgSb}_2$  ( $R = \text{Y, Sm, La}$ ) single crystals*, J. Phys.: Condens. Matter. 20 (2008), p. 115210. doi:10.1088/0953-8984/20/11/115210
- [36] E.C. dos Santos, E.F. da Silva, J.C. Fernandes, L. Ghivelder, D.C. Freitas, M.A. Continento, and L. Walmsley, *Non linear conduction due to depinning of charge order domains in  $\text{Fe}_3\text{O}_2\text{BO}_3$* , J. Phys.: Condens. Matter 29 (2017), p. 205401. doi:10.1088/1361-648X/aa6960
- [37] J.J. Larrea, D.R. Sánchez, F.J. Litterst, E.M. Baggio-Saitovitch, J.C. Fernandes, R.B. Guimarães, and M.A. Continentino, *Magnetism and charge ordering in  $\text{Fe}_3\text{O}_2\text{BO}_3$*



- studied by  $^{57}\text{Fe}$  Mössbauer spectroscopy, *Phys. Rev. B* 70 (2004), p. 174452. doi:10.1103/PhysRevB.70.174452
- [38] R. Weber and R. Street, *The heat capacity of chromium at 311 K (Antiferromagnetic to paramagnetic transition)*, *J. Phys. F: Metal Phys.* 2 (1972), pp. 873–877.
- [39] D.I. Bolef and J. De Klerk, *Anomalies in the elastic constants and thermal expansion of chromium single crystals*, *Phys. Rev.* 129 (1963), pp. 1063–1067. doi:10.1103/PhysRev.129.1063
- [40] M.B. Walker, *Phenomenological theory of the spin-density-wave state of chromium*, *Phys. Rev. B* 22 (1980), pp. 1338–1347. doi:10.1103/PhysRevB.22.1338
- [41] E. Fawcett, *Spin-density-wave antiferromagnetism in chromium*, *Rev. Mod. Phys.* 60 (1988), pp. 209–283. doi:10.1103/RevModPhys.60.209
- [42] W.L. McMillan, *Landau theory of charge density waves in transition-metal dichalcogenides*, *Phys. Rev. B* 12 (1975), pp. 1187–1196.
- [43] W.L. McMillan, *Theory of discommensurations and the commensurate-incommensurate charge density waves phase transition*. *Phys. Rev. B* 14 (1976), pp. 1496–1502.
- [44] W.L. McMillan, *Microscopic model of charge density waves in 2H – TaSe<sub>2</sub>*, *Phys. Rev B* 16 (1977), pp. 643–650.
- [45] D. Allender, J.W. Bray, and J. Bardeen, *Theory of fluctuation superconductivity from electron-phonon interactions in pseudo-one-dimensional systems*, *Phys. Rev. B* 9 (1974), pp. 119–129.
- [46] R.H. McKenzie, *Microscopic theory of the pseudogap and peierls transition in quasi-one-dimensional materials*, *Phys. Rev. B* 52 (1995), pp. 16428–16442.
- [47] F. Laliberté, M. Frachet, S. Benhabib, B. Borgnic, T. Loew, J. Porras, M. Le Tacon, B. Keimer, S. Wiedmann, C. Proust, and D. LeBoeuf, *High field charge order across the phase diagram of YBa<sub>2</sub>Cu<sub>3</sub>O<sub>y</sub>*, *npj. Quantum Mater.* 3 (2018), p. 411. doi:10.1038/s41535-018-0084-5
- [48] L. Landau and E. Lifshitz, *Statistic Physics*, Pergamon Press, 1968.
- [49] K. Binder, *Theory of first order phase transition*, *Rep. Prog. Phys.* 50 (1987), pp. 783–859. doi:10.1088/0034-4885/50/7/001
- [50] L.R. Testardi, *Elastic moduli, thermal expansion, specific heat at a phase transition*, *Phys. Rev. B* 12 (1975), pp. 3849–3854.
- [51] W. Rehwald, *The study of structural phase transitions by means of ultrasonic experiments*, *Adv. Phys.* 22 (1973), pp. 721–755.
- [52] B. Lüthi, *Solid-state-sciences, in Physical Acoustics in the Solid State*, M. Cardona, ed., Springer-Verlag, Berlin, 2005.
- [53] J.O. Fossum, *A phenomenological analysis of ultrasound near phase transitions*, *J. Phys. C: Solid State Phys.* 18 (1985), pp. 5531–5548.
- [54] A.M. Schorgg and F. Schwabl, *Theory of ultrasonic attenuation at incommensurate phase transitions*, *Phys. Rev. B* 49 (1994), pp. 11682–11703. doi:10.1103/PhysRevB.49.11682
- [55] A.D. Bruce and R.A. Cowley, *The theory of structurally incommensurate systems. III. The fluctuation spectrum of incommensurate phases*, *J. Phys. C: Solid State Phys.* 11 (1978), pp. 3609–3630.
- [56] P. Bak, *Commensurate phases, incommensurate phases and the Devil’s staircase*, *Rep. Prog. Phys.* 45 (1982), pp. 587–629.
- [57] H.Z. Cummins, *Experimental studies of structurally incommensurate crystal phases*, *Phys. Rep.* 185 (1990), pp. 211–409.
- [58] D.E. Moncton, J.D. Axe, and F.J. DiSalvo, *Neutron scattering study of the charge-density wave transitions in 2H – TaSe<sub>2</sub> and 2H – NbSe<sub>2</sub>*, *Phys. Rev. B* 16 (1977), pp. 801–819.



- [59] S. Manzeli, D. Ovchinnikov, D. Pasquier, O.V. Yazyev, and A. Kis, *2D transition metal dichalcogenides*, Nat. Rev. 2 (2017), p. 17033.
- [60] J. Wilson, F. Di Salvo, and S. Mahajan, *Charge density waves and superlattices in the metallic layered dichalcogenides*, Adv. Phys. 24 (1975), pp. 117–201. doi/10.1080/00018737500101391.